J. Biomedical Science and Engineering, 2010, 3, 1093-1098 **JBiSE**
doi:10.4236/jbise.2010.311142 Published Online November 2010 (http://www.SciRP.org/journal/jbise/).

Labeled Hepasphere™ behavior during venous drainage simulation at 1.5T*

Hassan Jassar, François Langevin

UMR6600-Centre of Advanced Medical Imaging, University of Technology of Compiegne, Compiegne, France.
Email: Hassan.jassar@utc.fr

Received 19 August 2010; revised 25 September 2010; accepted 30 September 2010.

ABSTRACT

Stability of the magnetic resonance (MR) contrast agent inside vascular occlusion agents is important for their localization with magnetic resonance imaging (MRI). The aim of this paper is to study the behaviour of the superparamagnetic iron oxide (SPIO) within Hepaspheres™ microparticles (MP) by *MRI* when they are submitted to negative pressure induced by venous drainage of a tumor. Therefore, a venous drainage model was established and three parameters were taken into account according to physiologic parameters in tumors: pH, temperature and flow blood rate. Four cycles of pumping were performed with the presence of labeled Hepaspheres™ with Endorem®. Several *MR* images of *MP* and perfusion liquid were taken before and after pumping. Endorem® release was determined after correction of non-uniformity intensities in *MR* images. Intensity variation according to spatial position, coil and *MR* acquisition parameters was studied. Labeled microparticles (LB*MP) appeared as black spots in *MRI* images whatever duration and pH. Our model demonstrates the stability of the *SPIO* inside the occlusion agent during time. Moreover, the proposed correction method proves the reduction of the intensity non-uniformity in *MRI* images.

Keywords: MRI; Venous Drainage Model; SPIO; Endorem®; Hepaspheres™; Intensity Non-Uniformity

1. INTRODUCTION

Embolization with *MP* consists in stopping blood flow and starving tissues of oxygen and nutrients [1]. For instance, Hepaspheres™ are dry *MP* in original state and become non-biodegradable microspheres after swelling within ionic fluids [2]. They are used as occlusion agents in hepatocellular carcinoma and arteriovenous malformations [3] and may release drugs *in situ* by diffusion [4]. Labelling these *MP* with superparamagnetic iron oxide (SPIO) to localize them has already been demonstrated [5]. However, the stability of *SPIO* within *MP* along time remains an important question, as a release of the contrast agent from *MP* could avoid the detection of their real position in clinical applications. Vessel occlusion provokes negative pressure on *MP*, especially with existing arteriovenous shunt around necrotic tissues or tumors [6,7].

Venous drainage model was performed in this work to determine *SPIO* behaviour within Hepaspheres™ by *MRI* during time. Several physiological factors of tumors were taken into consideration in the model: flow, temperature and pH. Simulation value of the flow was chosen much higher than standard one, as pessimistic conditions. This work included correction of the *MR* intensity non-uniformity for quantitative analysis reproducibility on *MR* images, leading to the estimation of released *SPIO* from the *MP*.

2. MATERIALS AND METHODS

2.1. Labelling Hepaspheres™ *MP* with Endorem®

SAP-MS (sodium acrylate and vinyl alcohol copolymer) or Hepaspheres™ provided by Biosphere Medical SA France were used as occlusion agents in hepatocellular carcinoma and arteriovenous malformations [2-4]. Particle sizes of Hepaspheres™ in dry state is calibrated in 50 µm increments ranging from 50 to 200 µm (50-100, 100-150 and 150-200 µm) [2]. Their diameters after swelling are approximately 2 to 3.5 times larger than their original size [8].

500 µl (25% v/v) of Endorem® was diluted into 1.5 ml (75% v/v) of saline solution. Solution was poured respectively into a bottle containing dry Hepaspheres™ of 150–200 µm size (Ref: V705HS). After two hours of Endorem® absorption, the preparation was then poured into a glass column with porous filter (porosity: 20 µm–

*This research was supported by the Centre of Advanced Medical Imaging at the University of Technology of Compiegne.

Flex 1.0 × 30 cm- Ref: 420401-1030). Labeled Hepaspheres™ with Endorem® were washed by gravity in this column: 10 ml of saline was added to the Hepaspheres™ during 15 minutes, to let saline leave entirely the column. The washing process was repeated four times.

A few *MP* were picked up and then fixed between two transparent gel layers of a Petri dish for using as a control (before pumping).

2.2. Venous Drainage Model

In vitro venous drainage model consisted of closed circuit and composed of a peristaltic pump (Ref. 40578 Fisher Bioblock Scientific), a thermostat bath (Julabo 5 liters, Ref: ED-5A/B) within immersed a glass column with porous filter (**Figure 1**). Labeled Hepaspheres™ with Endorem® were placed in the column and submitted to 20 ml of the saline. According to physiological parameters of hepatocarcinoma, flow rate of the peristaltic pump was adjusted to 10 ml/min, four times over-evaluated blood flow through hepatic tumor of 16g [6]; tow pH, 6.0 and 7.0, were used in this model. The thermostat bath was maintained at 37°C.

Four cycles of saline pumping was performed through the closed circuit, two hours per cycle. Every two hours, 10 ml of perfusion liquid was filled into vials to dose released *SPIO* by *MRI*. After each pumping cycle, some *LB*MP* were picked up from the glass column and dropped on a gel of a Petri dish, with *MP* control unsubmitted to pumping cycles.

Two pH solutions (6 and 7) were tested, providing eight vials of perfusion samples. A new 20 ml of the saline solution at one pH was added to the glass column after each pumping cycle.

MR scans were performed on GE Signa® 1.5T Excite™ 11.0 scanner. Quantitative analyses of all *MRI* images were done in our laboratory using an Advantage Windows (4.1-GE) workstation. Values averaging of signal intensities were performed with MATLAB® 7.0 and EXCEL® softwares.

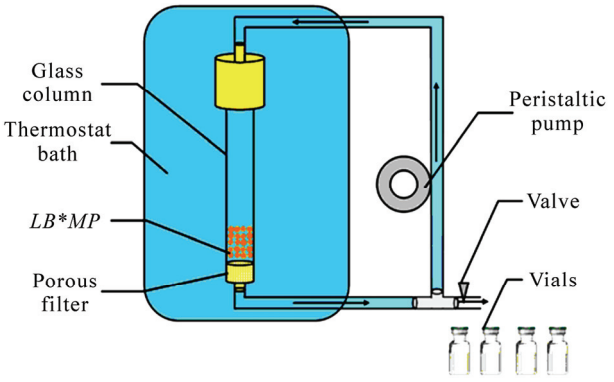

Figure 1. Simulation of venous drainage model with the presence of labeled Hepaspheres™. Perfusion liquid is filled into vials at the bottom right side of the schema.

2.3. Perfusion Liquid Imaging

Most intensity non-uniformities result from materials of the *MR* scanner such as coil, its sensitivity and the radiofrequency system [9-11]. Intensity non-uniformity correction methods may be classified into two types, as reported in literature [12]: empirical methods and post-processing techniques. Empirical methods involve scanning water or oil phantom prior to clinical examination [9,11,13,14] to obtain an estimate on the scanner's bias field. Post-processing techniques are the most commonly used approaches in the quantitative analysis of *MR* images [12,15-23]. These methods privilege modelling of the effects but not the cause of the intensity non-uniformities. Therefore, it is difficult to appreciate the pertinence of these methods.

The proposed method was a hybrid method taking advantage of the two categories: it first constituted a reference from an image of a phantom with given hardware and acquisition parameters. The independence of the sample location in the analysed region was searched by averaging the extracted values from phantom images after successive rotation of the phantom or the perfusion liquid.

2.3.1. Coil and Imaging Parameters

Volume coil (**Figure 2(c)**), such as head coil (diameter 30 cm and length 40 cm, one channel), *and* 2D *FSE-XL* T_1w were used in all *MR* acquisitions to provide low image-intensity non-uniformity [24-26]. Six contiguous slices were obtained in coronal plane with the imaging parameters: Repetition time/echo time = 500/15 ms, bandwidth = 15.63 kHz, field of view = 180 × 180 mm, matrix size = 128 × 128, slice thickness = 5 mm, number of signal average = 6, and echo train length = 4.

2.3.2. Reference Phantom and Intensities Averaging

A phantom composed of eight vials were uniformly filled with 10 ml of saline solution (0.9%), and equally distributed into two square matrices, matrix-1 and matrix-2 (**Figure 2(a)**). They were positioned on a rotating wooden support, equidistant from the coil centre with 5.6 cm of radius (**Figure 2(b)**). 45° is the angle between the two matrices and 8 cm is the distance between vials of the matrix. The ninth vial was in central position.

MR images of the phantom were acquired in four directions (superior «S», inferior «I», left «L» and right «R») after 90° of the support rotation. For this purpose, the phantom was brought out for each 90° rotation from the scanner without changing the support position inside the volume coil. Values of calibration in the first *MR* acquisition were kept the same after each «Prescan» for

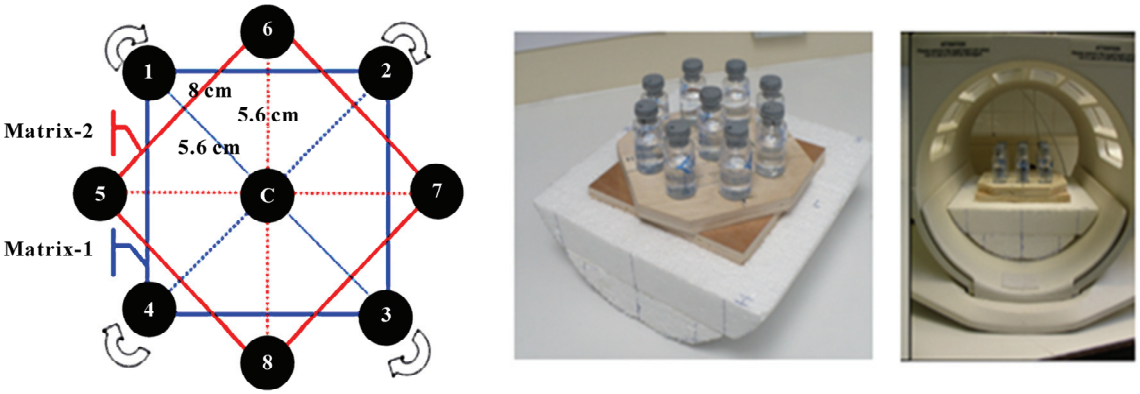

(a) (b) (c)

Figure 2. Schemas and photos of the saline solution phantom. (a) Eight vials were placed equidistantly to 5.6 cm from the centre «c» and distributed into two matrices: «matrix-1» and «matrix-2» at 45°. At centre «c», a ninth vial was common to the both matrices. (b) Glass vials were positioned on a rotating support of wood. (c) Fixed support of polystyrene carried vials on the wooden support to volume coil and tunnel centre.

the four directions.

Mean signal intensities of the four vials in the matrix-1 and matrix-2 were determined for a given direction. Dissimilarity of intensity values in the *MR* images could be an indicator of the percentage of intensity non-uniformity resulting from vials neighboring.

Intensity non-uniformity correction by signal averaging of the same vial was performed in the four directions after successive rotation of the phantom support.

The pertinence of this method was evaluated according to Wicks' formula [11]:

$$G = \frac{\sigma}{\mu} \times 100 \quad (1)$$

where (G) is the percentage of non-uniformity, (σ) is the standard deviation of the sample vial intensities in the *MR* image and (μ) their mean.

Therefore, percentage of non-uniformity was calculated before (G) and after averaging ($\overline{G}$).

2.3.3. Perfusion Liquid and Intensities Averaging

Eight vials of perfusion liquid were placed on the support equidistantly from the coil centre, and distributed into two matrices, «matrix-1» for pH7 and «matrix-2» for pH6 at 45°. The ninth vial containing intact saline solution was common to both matrices. Perfusion liquid imaging was performed likely to phantom acquisitions to determine signal intensities μ of vials on T_1w image. Intensities averaging $\overline{\mu}$ were performed for each vial (pH6 and pH7) of the two matrices, in the four directions. Then, contrast between signal intensities of samples and saline solution was determined according to equation:

$$\frac{\overline{\mu}_{perfusion-liquid} - \overline{\mu}_{saline}}{\overline{\mu}_{perfusion-liquid} + \overline{\mu}_{saline}} \quad (2)$$

3. RESULTS

3.1. Hepaspheres™ Imaging

Figure 3 shows T_1w images of two Petri dishes plunged into water and containing labeled Hepaspheres™ with *SPIO*. *LB*MP* submitted to pumping cycles (2h, 4h, 6h and 8h) remains visible on *MR* images as black spots whatever pumping time and pH of saline. This result was similar to that of *LB*MP* unsubmitted to pumping cycles (0h). This means that Endorem® was unreleased or slightly released without affecting the signal intensity of labeled *LB*MP*. Determined intensities of perfusion liquid provide more information on a trace of *SPIO* that possibly released from *LB*MP*, as shown in Subsection 3.3.

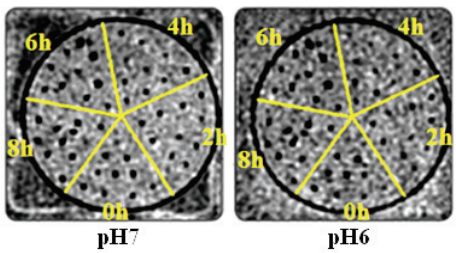

Figure 3. T_1w images of Petri dishes after being plunged in water. These contained labeled Hepaspheres™ with Endorem® that submitted to four cycles of pumping at pH7 (left) and pH6 (right). *MR* images were acquired in coronal plane with 3*D SPGR* T_1w acquisition of parameters: TR/echo time = 35/5 ms, flip angle = 45°, field of view = 140 × 140 mm, slice thickness = 1 mm, number of slices = 28, matrix size = 256 × 256, bandwidth = 15.63 kHz and Nex = 1. Imaging was realized with the use of a surface coil (phased array, 4 channels).

3.2. Phantom Imaging and Averaging Intensities Evaluation

Figure 4(a) is T_1w image of the phantom whose vials are equidistantly distributed from the centre «c». **Figure 4(b)** shows clearly the influence of neighbors proximity on the signal intensity. Percentage difference between mean signal intensities of «matrix-1» and «matrix-2» is significant in the four directions (**Table 1**).

Figure 5 shows a non-uniformity percentage variation of intensities G versus vial positions and phantom directions, before and after averaging. Before averaging, G variation is important. It is less significant after averaging (**Figure 5(a)**, green curves). 0.094 is the average absolute deviation of $\overline{G}$ (**Figure 5(b)**). This value means low intensity non-uniformity for the equidistant distribution of vials on the support.

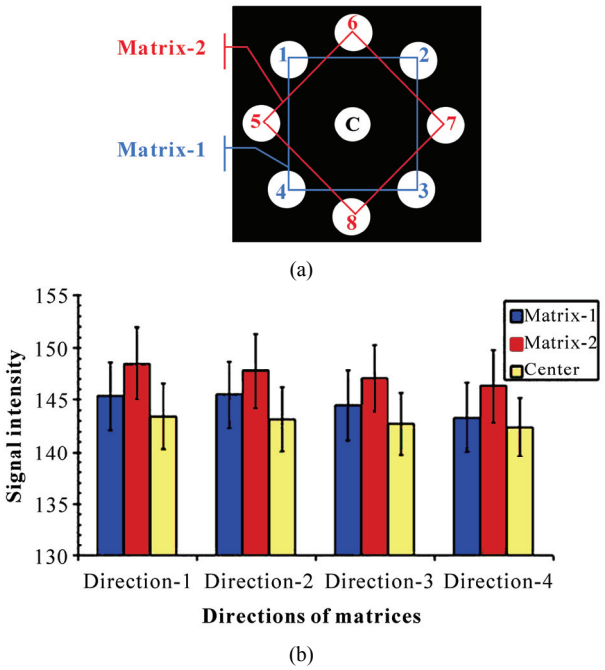

Figure 4. T_1w images of a saline phantom acquired by FSE-XL T_1. (a) *MR* images of eight vials equidistantly distributed from the centre «C» into two matrices: «matrix-1» and «matrix-2» at 45°. (b) Vials' intensities of matrix-1, matrix-2 and saline solution at the centre, in the four directions.

Table 1. Percentage difference between averaged intensities of «matrix-1» against «matrix-2» at 45° according to vials' positions and directions for a phantom of saline solution.

Directions	% difference of vial's intensities
1	2,19%
2	1,56%
3	1,75%
4	2%

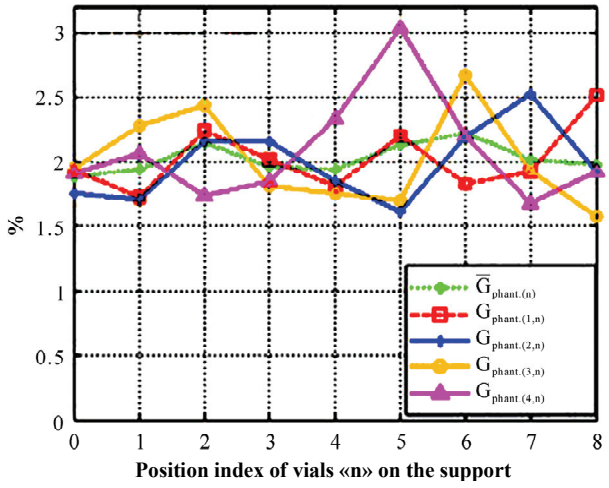

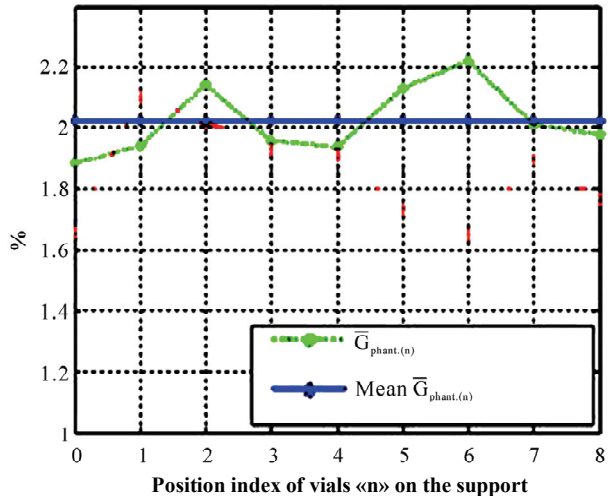

Figure 5. (a) Non-uniformity percentage of signal intensities (%) determined on each vial (n = 0 to 8) of the saline phantom before ($G_{phant.(i,n)}$, red, blue, yellow and pink colours) and after averaging ($\overline{G}_{phant.(n)}$, green colour). The point 0 corresponds to the non-uniformity percentage of signal for a vial in the central position. (b) Average absolute deviation of non-uniformity percentage averaging ($\overline{G}_{phant.(n)}$) against mean of $\overline{G}_{phant.(n)}$ for each element of the phantom. Zero point corresponds to the vial in common to the two matrices.

3.3. Perfusion Liquid Signal

The signal at pH7 is greater than that of saline solution at the two first cycles of pumping, 2h and 4h. 22% is the percentage of the signal decrease between 2h and 6h of pumping time, then the signal becomes stable (**Figure 6**). 15% at 2h and 6% at 4h are the contrast of perfusion liquid-saline solution; it is almost zero at 6h and 8h of pumping time.

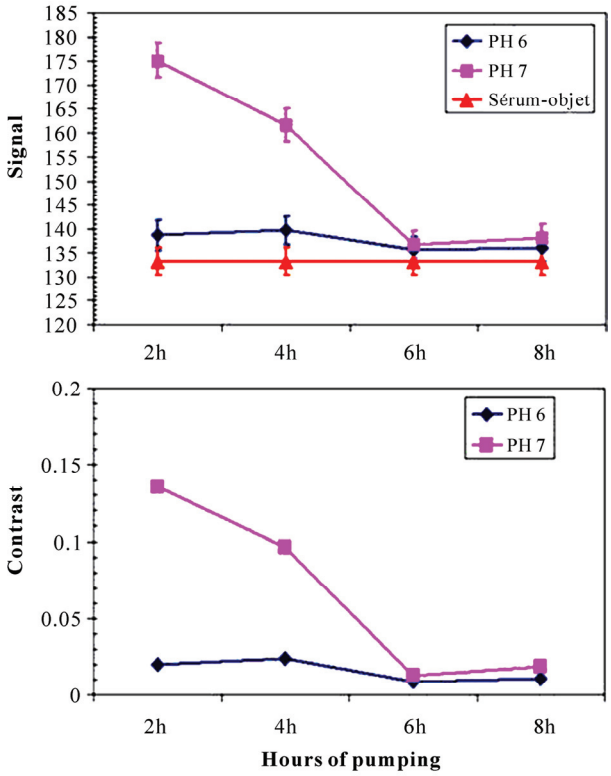

Figure 6. Representation of perfusion liquid signal (right) and liquid-saline contrast (left) in function of hours of pumping, at pH6 and pH7. Each signal value was averaged in the four directions.

When the signal of perfusion liquid is greater than that of saline solution the contrast is important, proving that Endorem® has been slightly released from Hepaspheres™. However, when the signal is equivalent to that of saline solution, the contrast becomes zero after 6h of pumping time. Therefore, the Endorem® release does not exist.

The signal of perfusion liquid at pH6 after eight hours of pumping is close to that of saline solution. 3% is the contrast of perfusion liquid against saline solution. This means an absence of Endorem® in the perfusion liquid during all pumping time.

4. DISCUSSION

For the three physiological parameters values of hepatocellular carcinoma, pH, temperature and flow rate, we demonstrated that the labeled Hepaspheres™ with Endorem® could be detected by *MRI* in the proposed conditions. These are visible in conventional *MRI* (1.5T) as black spots (negative contrast or low signal) and distinguished from the surrounding signal of gel whatever the hours of pumping and the pH.

Perfusion liquid-saline contrast difference between pH7 and pH6 is 14.8% at 2h and 11.5% at 4h of pumping. It then becomes 2.5%. This implies a release of Endorem® from Hepaspheres™ in the first hours of pumping, only at pH7.

Then, releasing reaches the stability when the signal of perfusion liquid becomes very close to that of saline solution. This can be demonstrated by zero release of the contrast agent after several hours of pumping, although, Hepaspheres'™ properties let drug absorption and delivery. This observation may be depending on the spongy behaviour of Hepaspheres™. Very low release of Endorem® at pH6 shows that the behaviour of Hepaspheres™ could be modified by pH decreasing.

For the proposed intensity non-uniformity correction method and the distribution of vials to the volume coil centre, we demonstrated that the average absolute deviation of the non-uniformity percentage was 0.094.

This method reduced the intensity non-uniformities in function of position, coil and acquisition parameters, and provided an accurate measure of the perfusion liquid signal. Consequently, quantification of released Endorem® could be determined precisely.

Finally, we noticed that the preliminary process of four hours of pumping provides visible Hepaspheres™ in *MRI* images.

This study determines the behaviour of labeled Hepaspheres™ with Endorem® when submitted in a venous drainage model to negative pressure and some physiological parameters of Hepatocarcinoma. Using 1.5T scanner for Hepaspheres™ imaging demonstrates a permanent *MR* detection of Hepaspheres™ whatever the proposed conditions that can be found nearly to tumors. This result provides stable labeled Hepaspheres™ with *SPIO* for using in *MR* interventional application.

5. ACKNOWLEDGEMENTS

Authors thank Philippe Robert of Guerbet for providing the SPIO. We thank Philippe Reb of Biosphere Medical for providing Hepaspheres™.

REFERENCES

[1] Laurent, A., Wassef, M., Chapot, R., Wang, Y., Houdart, E., Feng, L., Tran Ba Huy, E. and Merland, J.J. (2005) Partition of calibrated tris-acryl gelatin microspheres in the arterial vasculature of embolized nasopharyngeal angiofibromas and paragangliomas. *Journal of Vascular and Interventional Radiology*, **16(4)**, 507-513.

[2] Osuga, K., Hori, S., Kitayoshi, H., Khankan, A., Okada, A., Sugiura, T., Murakami, T., Hosokawa, K. and Nakamura, H. (2002) Embolization of high flow arteriovenous malformations: Experience with use of superabsorbent polymer microspheres. *Journal of Vascular and Interventional Radiology*, **13(11)**, 1125-1133.

[3] De Luis, E., Bilbao, J.I., de Ciércoles, J.A.G.J., Cuesta, A. M., Rodríguez, A.M. and Lozano, M.D. (2008) In vivo evaluation of an new embolic spherical particle (HepaSphere) in a kidney animal model. *Cardiovascular and*

Interventional Radiology, **31(2)**, 367-376.

[4] Osuga, K., Khankan, A.A., Hori, S., Okada, A., Sugiura, T., Maeda, M., Nagano, H., Yamada, A., Murakami, T. and Nakamura, H. (2002) Transarterial embolization for large hepatocellular carcinoma with the use of superabsorbent polymer microspheres: initial experience. *Journal of Vascular and Interventional Radiology*, **13(9)**, 929-934.

[5] Jassar, H. (2009) Detectability of vascular occlusion materials for MRI follow-up. Ph.D. Dissertation, Compiegne University of Technology, Compiegne.

[6] Vaupel, P., Rallinowski, F. and Okunieff, P. (1989) Blood flow, oxygen and nutrient supply, and metabolic microenvironment of human tumors: A review. *Cancer Research*, **49(23)**, 6449-6465.

[7] Tancredi, T., McCuskey, P.A., Kan, Z. and Wallace, S. (1999) Changes in rat liver microcirculation after experimental hepathic arterial embolization: Comparison of different embolic agents. *Radiology*, **12(1)**, 117-181.

[8] Khankan, A.A., Osuga, K., Hori, S., Morii, E., Murakami, T. and Nakamura, H. (2004) Embolic effects of superabsorbent polymer microspheres in rabbit renal model: comparison with tris-acryl gelatin microspheres and polyvinyl alcohol. *Radiation Medicine*, **22(6)**, 384-390.

[9] Simmons, A., Arridge, S.R., Barker, G.J. and Williams, S.C. (1994) Sources of intensity nonuniformity in spin echo images at 1.5 T. *Magnetic Resonance in Medicine*, **32(1)**, 12-18.

[10] Haacke, E.M., Brown, R.W., Thompson, M.R. and Venkatesan, R. (1999) Magnetic resonance imaging. *Physical Principles and Sequence Design*, Wiley-Liss, New York.

[11] Wicks, D.A.G., Barker, G.J. and Tofts, P.S. (1993) Correction of intensity nonuniformity in MR images of any orientation. *Magnetic Resonance Imaging*, **11(2)**, 183-196.

[12] Zhou, L.Q., Zhu, Y.M., Bergot, C., Laval-Jeantet, A.M., Bousson, V., Laredo, J.D. and Laval-Jeantet, M. (2001) A method of radio-frequency inhomogeneity correction for brain tissue segmentation in MRI. *Computerized Medical Imaging and Graphics*, **25(5)**, 379-389.

[13] Axel, L., Constantini, J. and Listerud, J. (1987) Intensity correction in surface-coil MR imaging. *American Journal of Roentgenology*, **148**, 418-420.

[14] Simmons, A., Arridge, S.R., Barker, G.J., Cluckie, A.J., and Tofts, P.S. (1994) Improvements to the quality of MRI cluster analysis. *Magnetic Resonance Imaging*, **12(8)**, 1191-1204.

[15] Styner, M., Brechbuhler, C., Szekely, G. and Gerig, G. (2000) Parametric estimate of intensity inhomogeneities applied to MRI. *Medical Imaging*, **19(3)**, 153-165.

[16] Lai, S.H. and Fang, M. (1999) A new variational shape-from-orientation approach to correcting intensity inhomogeneities in magnetic resonance images. *Medical Image Analysis*, **3(4)**, 409-424.

[17] Pham, D.L. and Prince, J.L. (1999) A generalized EM algorithm for robust segmentation of magnetic resonance images. 33*rd Annual Conference on Information Sciences and Systems*, Baltimore, 558-563.

[18] Narayana, P.A. and Bourthakour, A. (1995) Effect of radio frequency inhomogeneity correction on the reproducibility of intra-cranial volumes using MR image data. *Magnetic Resonance in Medicine*, **33(3)**, 396-400.

[19] Vorkurka, E.A., Thaker, N. and Jackson, A. (1999) A fast model independent method for automatic correction of intensity nonuniformity in MRI data. *Journal of Magnetic Resonance Imaging*, **10(4)**, 550-562.

[20] Brinkmann, B.H., Manduca, A. and Robb, R.A. (1998) Optimized homomorphic unsharp masking for MR grayscale inhomogeneity correction. *IEEE Medical Imaging*, **17(2)**, 161-171.

[21] Likar, B., Viergever, M.A. and Pernus, F. (2000) Retrospective correction of MR intensity inhomogeneity by information minimization. *MICCAI Conference on Medical Image Computing and Computer-Assisted Intervention*, **1935/2000**, Pittsburgh, 375-384.

[22] Cohen, M.S., DuBois, R.M. and Zeineh, M.M. (2000) Rapid and effective correction of RF inhomogeneity for high field magnetic resonance imaging. *Human Brain Mapping*, **10(4)**, 204-211.

[23] Han, C., Hatsukami, T.S. and Yuan, C. (2001) A multi-scale method for automatic correction of intensity non-uniformity in MR images. *Proceedings of International Society for Magnetic Resonance in Medicine*, **13(3)**, 428-436.

[24] Hayes, C.E., Edelstein, W.A., Schenck, J.F., Otward, M. M. and Eash, M. (1985) An efficient, Highly Homogeneous Radiofrequency Coil for whole-body NMR Imaging at 1.5 T. *Journal of Magnetic Resonance*, **63**, 622-628.

[25] Simmons, A., Tofts, P.S., Barker, G.J. and Arridge, S.R., (1994) Sources of intensity non uniformity in spin echo images at 1.5T. *Magnetic Resonance in Medicine*, **32(1)**, 121-128.

[26] Barker, G.J., Simmons, A., Arridge, S. R. and Tofts, P.S., (1998) A simple method for investigating the effects of non-uniformity of radiofrequency transmission and radiofrequency reception in MRI. *The Britch Journal of Radioliogy*, **71(841)**, 59-67.

